Int J Adv Manuf Technol (2014) 75:1103–1113
DOI 10.1007/s00170-014-6197-5

ORIGINAL ARTICLE

Experimental analysis of damage propagation in riveted CFRP-steel structures by thermal loads

Julia Wagner · Maximilian Wilhelm · Horst Baier · Uwe Füssel · Thomas Richter

Received: 13 January 2014 / Accepted: 22 July 2014 / Published online: 13 August 2014

Abstract This paper focuses on the description of damage propagation around rivets in multiple joined single lap carbon fiber reinforced plastics (CFRP)-steel structures due to loads as a consequence of different coefficients of thermal expansion. Materials and rivets were chosen according to automotive body shop applications. Specimens were evaluated non-destructively in ultrasonic C-scans to characterize damage behavior of blind and self-piercing rivets in CFRP-steel-connections before and after the application of thermal loads. An algorithm for an automated detection of damage size on ultrasonic C-scan images was developed as the basis for further damage classification. The results show that blind riveting (BR) causes crack-like initial damage that broadens to roundish plane defects due to heating. Initial extensive damage due to self-piercing riveting (SPR) propagates in elliptic shape. Additionally, tension tests revealed a loss in ultimate load by 10–15 % induced by thermal loads and associated with damage propagation. A correlation between initial damage, relative displacement, and thermal loads was observed.

J. Wagner · M. Wilhelm (✉) · T. Richter
Joining Technique Body Shop, BMW Group, Landshuter Str. 56, 84130 Dingolfing, Germany
e-mail: maximilian.f.wilhelm@bmw.de

H. Baier
Institute of Lightweight Structures, Technische Universität München, Boltzmannstr. 15, 85748 Garching, Germany

U. Füssel
Institut für Fertigungstechnik, Professur Fügetechnik und Montage, Technische Universität Dresden, George-Bähr-Str.3c, 01069 Dresden, Germany

Keywords Joining · Fiber reinforced composites · Blind riveting · Self-piercing riveting · Mixed material applications · Thermal loads

1 Introduction

Modern automotive body constructions combine fiber composite and metal parts to create light and stiff functional structures. Connecting CFRP and metal components usually involves joining methods like riveting, bolting, screwing, or adhesive bonding. The respective joining process is chosen according to cost, quality, and production cycle time. The requirements of the automotive industry regarding these criteria, however, differ strongly from those of the space and aircraft industry, where CFRP-components have a longer tradition. Automotive applications of fiber compounds are designed to satisfy a high degree of automation. Compared to the space and aircraft industry, it is therefore necessary to widen part and material tolerances, to use resource efficient as well as robust production processes and cycle time optimized joining techniques, to turn out high quantities. Blind and self-piercing riveting are widespread techniques in automotive fastening for mixed material connections of steel and aluminum, therefore experience and detailed process comprehension are available. Reviews by [2], [18], and [9] give examples of the state of the art regarding these joining techniques for automotive applications. Hence, those two processes are chosen to show their suitability for multi-material body structures containing CFRP. The first challenge arises from the inducement of delaminations and inter-fiber breakages during pre-hole preparation or joining [21]. These imperfections are caused by the self-piercing or drilling process as well as the deformation energy necessary

for the formation of the joint. In [15], only an influence of said imperfections on 4 % design bearing strength is shown and in [20] no influence at all of different amounts of imperfections on ultimate strength is observed. The integration of fiber composite materials in the classic process chain of the automotive industry, containing cathodic dip painting with process temperatures up to $180°C$, however, comes with further challenges. Especially the relation between translational displacement in the area of the fixation, induced by the differing coefficients of thermal expansion α, and the correlating damage propagation need to be investigated (see Fig. 1). In contrast to the challenges of imperfections in the immediate vicinity of joints and translational displacement due to heating processes, the knowledge on bolted CFRP-connections in general is broad. Good reviews on the topic are given by [4, 19].

Some researchers have studied thermal residual stresses and damage behavior in mixed material applications for adhesive joints [11, 12, 14, 16]. But only little research is known on the topic of riveted joints. In pioneering work, [7] shows the challenges of thermal loads in mixed material applications on a riveted picture frame specimen. A detailed analysis of damage propagation in hybrid joints however is not investigated. Nevertheless, literature analyzing bolted joints under different thermal environment exist. In [6], for example, progressive failure is studied in tension tests on bolted joints under different thermal environments and different failure criteria are compared in a simulation. Clearly, the focus of the paper is the prediction of failure load rather than the propagation and description of damages around hole edge. The correlation between interlaminar stress peaks and damaged areas under different thermal environments is investigated by [22] for pin-loaded specimens. Bearing strength is considered to be a function of thermal dependent material properties and changes in residual stresses [22]. However, only a little research is discussed in the literature focusing on mixed material applications joined with rivets undergoing internal thermal loads due to different thermal elongation coefficients. Accordingly, the objective of this paper is to describe and characterize damage propagation on CFRP-steel structures by thermal expansion joined with blind and self-piercing rivets.

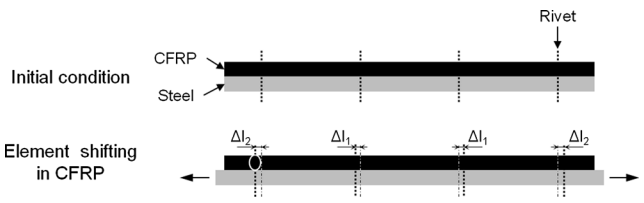

Fig. 1 Element shifting in mixed material constructions under thermal expansion

2 Theory

The developed theory was verified using a highly anisotropic laminate manufactured in resin transfer molding from two layers of braided carbon/glass fiber hybrid material and an epoxy resin joined with a stiff steal profile. For detailed information on the materials see Table 1.

The specimen geometry was adapted to ensure a certain length between the outermost joining points and to allow therefore a certain expansion of the steel (see Fig. 2). The assembly itself is not shaped completely symmetrically, since the specimen is designed to fit for both, tension tests and damage initiation through thermal elongation. The contact surface between CFRP and steel however is built symmetrically in relation to the center of the two inner rivets to ensure symmetric elongation conditions at the joints as far as possible.

The steel partner of type CR240BH was chosen as a u-profile with a thickness t=1.5 mm to build a specimen that is much less susceptible to bending than flat blanks. In order to clamp the specimens for tension tests, the u-profile was straightened up at one end. A finite element analysis of the deformation under thermal load was conducted for the steel specimen for a temperature difference $\Delta T = 157\ K$ to cover the range between room temperature ($23°C$) and maximum process temperature of the paint shop ($180°C$). The steel part showed less than 0.05 mm out of plane displacement in the area of the four joining points. As only insignificant bending of the specimens could be observed the specimen geometry proofed to be usable for further research. The specimens were joined by standard blind rivets and semi-tubular self-piercing rivets as given in Table 2.

Testing was done in displacement control at a rate of 10 mm/min using a testing machine of type Zwick XC-FR250SN with an integrated 250 kN load cell. For evaluation of imperfections induced by riveting or thermal loads, ultra sonic testing in immersion technique was used, based on the findings of [13] and [23]. To ensure highest quality of inspection, a point focused transceiver was employed. Thermal loads were applied by heating the specimens in an oven for 20 min at 180 °C to simulate the conditions of cathodic dip painting in automotive industry. Therefore, the parts were left in the oven during heating and cooling in order to reproduce a temperature profile that is typical for the painting process chain in the automotive industry. All experiments have been carried out for both blind and self-piercing rivets. Nondestructive inspection was performed for each specimen after manufacturing and after thermal loads had been applied. To detect final failure behavior, all specimens were evaluated in a force/displacement measurement, see Fig. 3.

Table 1 Mechanical properties of the CFRP and the steel

Material	Elastic modulus [GPa]	Tensile strength [MPa]	Coefficient of thermal expansion $[10^{-6} \cdot K^{-1}]$	Thickness [mm]
CFRP (braided) $(\pm 45° G/0° C)_s$	$E^{\|\|} = 84$ $E^{\perp} = 9$	$R_m^{\|\|} = 1,141$ $R_m^{\perp} = 44$	$\alpha^{\|\|}(23°C) = -0.677$ $\alpha^{\|\|}(180°C) = -0.445$	2.1
Steel	$E = 210$	$R_m = 377$	$\alpha(23°C) = 12$ $\alpha(180°C) = 13$ according to [17]	1.5

2.1 Specimen behavior under thermal loads

While exposing joined materials with different coefficients of thermal expansion to heat, the deformation is always restricted by a differing expansion behavior, which leads to internal stresses. Thermal expansion of the specimen components, without considering the joining constraints, leads to a relative displacement of the joining points to a thought point of origin in the middle of the two central rivets. The distance between the position of a joint in the specimen at maximum temperature to the initial position at room temperature is seen as an equivalent for the delocalization that would occur without exposing the specimens to the geometric constraints of joining (see formulas 1, 2 and 3). The calculated values for ΔL are used to set the damage on the joints in relationship to their position on the specimen. For the specimen geometry of Fig. 2, bearing failure is, according to [8], expected to be dominant due to a low ratio of specimen width to hole diameter as well as due to low ratios of edge distance to hole diameter. The rivet is assumed to be pulled through the fiber composite depending on the displacement equivalent, whereby induced internal stresses are reduced. Thus, low values for ΔL are an indicator for small scale damage while joints with a higher ΔL tend to show larger damaged areas. This theory is valid as long as bearing failure, which is understood as the irreversible deformation around the hole due to a joining element under load pressing against the hole edge according to [1], is dominant.

$$\Delta L_{mat} = L_{(23\,^{\circ}\mathrm{C}),mat} - L_{(180\,^{\circ}\mathrm{C}),mat} \tag{1}$$

$$= \epsilon_{mat} \cdot L_{(23\,^{\circ}\mathrm{C}),mat} \tag{2}$$

$$= L_{(180\,^{\circ}\mathrm{C}),mat} \cdot \alpha_{mat}(T_{(180\,^{\circ}\mathrm{C})} - T_{(23\,^{\circ}\mathrm{C})}) \tag{3}$$

where ϵ is the elongation due to thermal expansion; $L(T)$ is the length at T; T is the temperature; and α is the coefficient of thermal expansion.

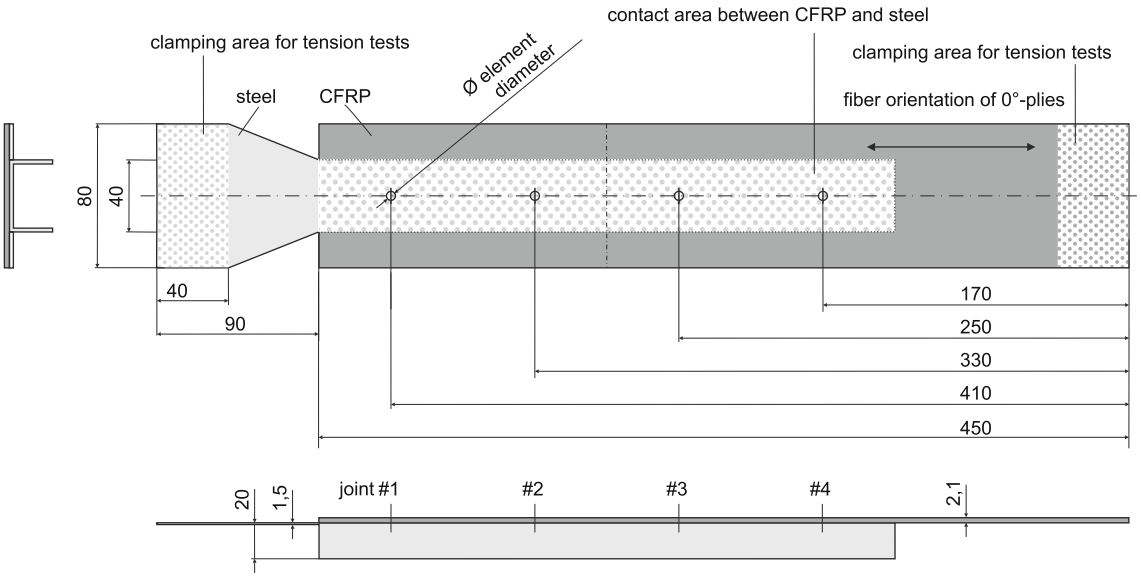

Fig. 2 Specimen geometry consisting of a CFRP plate and a steel u-profile

Table 2 Blind- and self-piercing rivets used for manufacture of joints

Technique	Element manufacturer	Element type	Element diameter [mm]
Blind riveting (BR)	RIBE	Wiredraw	4.8
Self-piercing riveting (SPR)	Böllhoff	Countersunk head	5.3

The combined translational displacement equivalent for both components of the specimen due to differing coefficients of thermal expansion can be calculated after formula (4).

$$\Delta L = \Delta L_{Steel} - \Delta L_{CFRP} \tag{4}$$

Using the temperature depending coefficient of thermal expansion ΔT of the used CFRP, a shrinkage less than 0.009 % in main fiber direction (0°-direction) was calculated for $\Delta T = 157K = T_{(23\,^\circ\mathrm{C})} - T_{(180\,^\circ\mathrm{C})}$ according to [5] after formula (3).

$$L(T) = L(T_0) \cdot e^{\int_{T_0}^{T} \alpha(T) dT} \tag{5}$$

where T_0 is the room temperature. For the steel specimen, the coefficient of thermal expansion was calculated as a mean value of a linear curve in the given temperature range to $\alpha(T)_{Steel} = 12.5 \cdot 10^{-6} K^{-1}$ according to [3]. The translational displacement for the two outer (see Fig. 2, joints #1 and #4) and for the two inner points (see Fig. 2, joints #2 and #3) is assumed to be symmetric starting between the two central rivets. The maximum relative displacement equivalent ΔL can therefore be calculated to 0.25 mm for the two outer and 0.08 mm for the two inner joints. Since the used CFRP tends to shrink due to heat, the total relative displacement equivalent, calculated with formula (4), is slightly larger than the sole steel elongation of 0.24 mm. The relative displacement equivalent ΔL can be seen as a simple calculable value to link the damage on the CFRP part to the position of the joints where the damage is initiated and propagates. The stress analysis, however, is much more comprehensive due to complex geometrical and mechanic conditions. When examining the stresses in the CFRP through thermal loads, three major influencing variables have been identified:

1. Outer constraints due to the four rivet joints and the inflexible and stiff steel part that restrict the movement of the CFRP part
2. Production induced internal stresses in the CFRP
3. Highly anisotropic material behavior of the braided CFRP

An analysis of the resulting strains and stresses in the specimen needs to take the above noted criteria into account so that the detailed study on the stresses is out of the scope of this paper. Specimen weight was measured before, during, and after the heating process to study the possibility of moisture absorption. As the weight changed less than 0.3 % in relation to the first measurement directly after riveting, additional effects of moisture are not considered in this research. For a stress analysis, however, moisture absorption has to be taken into account, since a therefore changed bearing strength and different internal stresses are influencing the material behavior in the thermal process [10].

2.2 Automated damage detection and evaluation

For the evaluation of the measured ultrasonic signals, an automated evaluation algorithm was developed. Starting with the graphical output of the C-scan, the algorithm detects damaged areas by assigned colors. Moreover, those defects are measured in maximum length and height as well as in total area. Besides the rivet center is detected and damage can be analyzed according to its propagation direction. The obtained data, including a comparison of the processed images and measured values, is subsequently printed to the analysis. The image processing algorithm was built in MATLAB and can be operated by a graphical user interface. The sequence of the single process steps is shown in a flowchart (see Fig. 4). The program requires

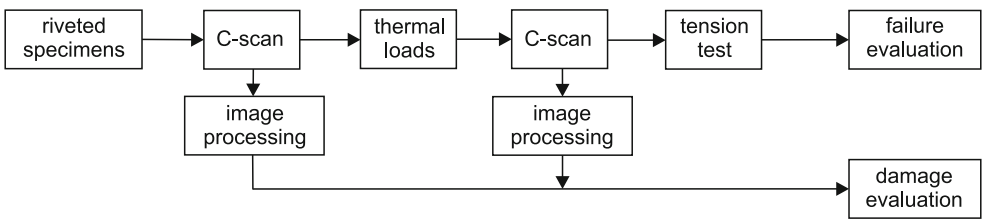

Fig. 3 Flow diagram of the test procedure

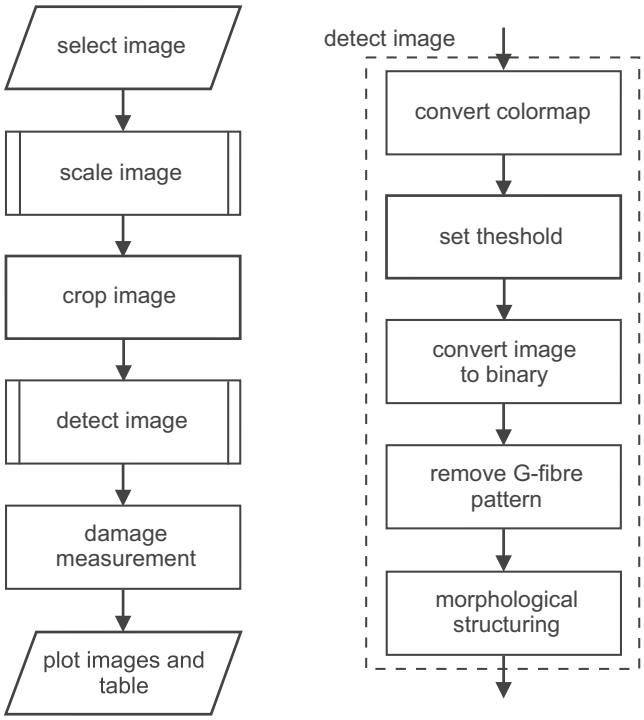

Fig. 4 Flow chart for automated image processing

colored image data obtained in a nondestructive inspection of the specimen. Containing data about signal-strength and therefore also included damage, the digital image provides information on the condition of the tested CFRP. Using a graphical user interface, the image can be rescaled and calibrated on a reference unit. Moreover, areas can be cropped to eliminate external disturbance. Subsequently, the image data is computed to a binary image through a separation of an experience gained threshold value for the boundary of a damaged area. Since glassfibers create a pattern of interfering signals in the ultrasonic image, the algorithm is taught to remove those flaw locations, whereby sensitivity for small damaged areas depends on the distance to large-area damage. The resulting black and white image is measured in area and dimensions depending on the main fiber direction. The acquired data of damaged zones is manually postprocessed to identify damage behavior of blind and self-piercing rivets in CFRP. Therefore, area and total dimensions of the bounding box parallel to the main fiber direction are evaluated. The length of the bounding box can consequently be seen as the longitudinal damage expansion l and is a indicator for the shape of the damage when set in relation to the measured damage area A, as used in Section 3.1 of this paper.

The developed algorithm also enables an automatic detection of the rivet center by using circular Hough transformation of filtered images. This function allows a calculation of damaged area spread related to the rivet center points. The direction of propagation can therefore be visualized automatically for each joint.

3 Results and discussion

Results from the automatic damage evaluation are shown in Fig. 5. Longitudinal (0°-direction) and transversal (90°-direction) dimensions as well as the damaged area were measured at four points on each of ten specimens for blind and self-piercing rivets (see Fig. 2, joints #1 to #4). It is evident that for blind and self-piercing riveting the detected damage differs in shape and dimensions. Since the used self-piercing rivets punch the CFRP with 7 kN and bend fibers circular into the sheet plane, initial damage is already visible without using nondestructive inspection methods.

The damaged contour is mostly elliptical in shape, whereby the orientation of the CFRP influences the direction of the longitudinal oval axis. The placement of blind rivets in holes leads to cracks and smaller area damage due to bearing stress caused by the widening rivet sleeve. The investigations have shown that the total damaged area caused by self-piercing rivets is almost one and a half times the size of the damage produced by the blind rivets, even though both have about the same nominal diameter.

3.1 Detected damage and damage propagation

Immediately after riveting, the identified damage in the CFRP caused by the blind rivets is evenly distributed between all four joints of the specimen (see Fig. 6). At this stage, the fiber composite is already pre-damaged by hole drilling and this failure increases through bearing stresses at the contact surface between borehole and rivet body. A specific crack-like shape of the damaged area can be identified for blind riveting. The rivet's clamping force is applied through freezing sleeve widening and therefore local hole bearing and expansion is provoked. Crack propagation starting at hole edge can be observed especially in main fiber direction since the used CFRP has no 90°-layer to stop these flaws.

Since bearing failure is the dominant failure mechanism according to [8], the rivet is assumed to be pulled through the fiber composite depending on the displacement equivalent. Due to a smaller relative displacement equivalent ΔL at the two central rivets, bearing failure is significantly less, which is also reflected in an evaluation of ultrasonic measurements. Damaged area increases for all four bolts, whereby for the outer rivets more damage is caused compared to those in the center, due to a larger ΔL on the edge of the specimen. Investigations have shown that growth normal to main fiber direction does not differ significantly

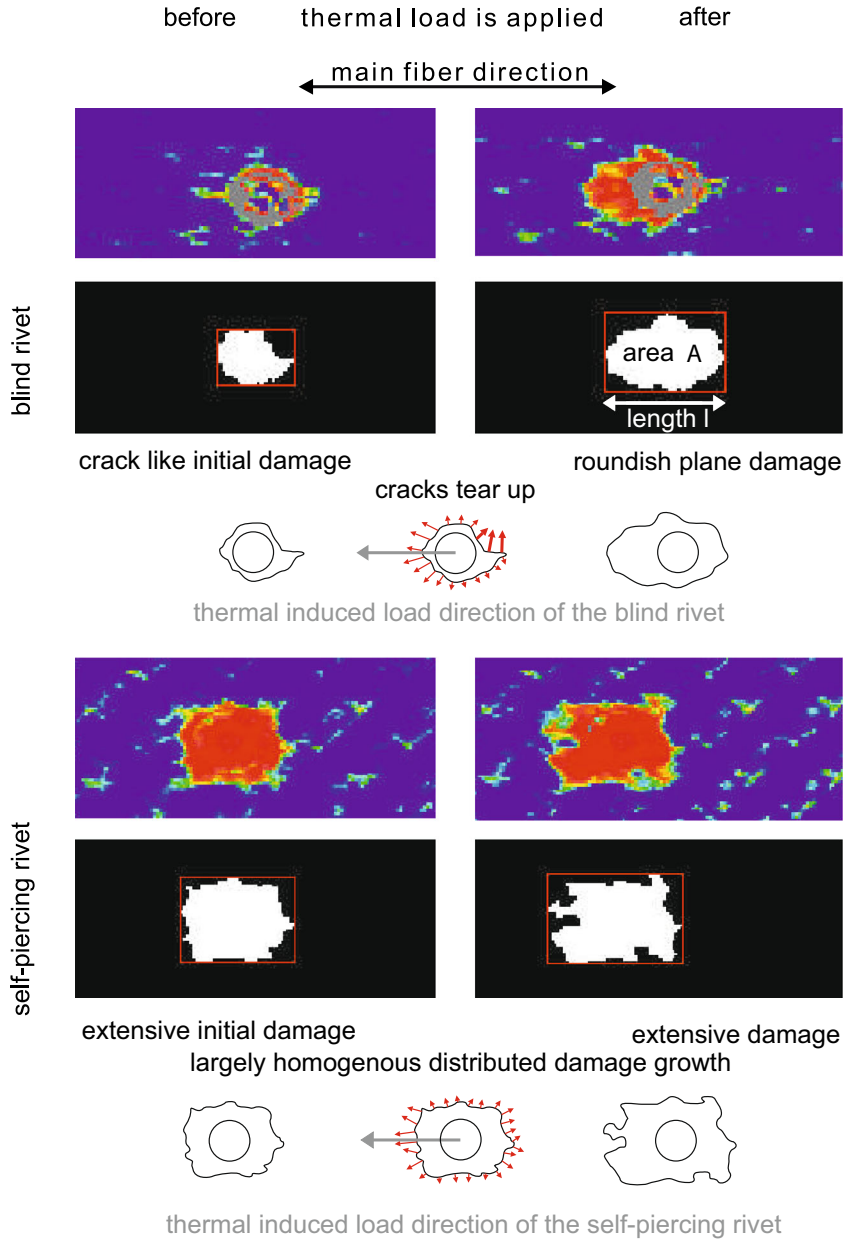

Fig. 5 Processed C-scan images before and after thermal load

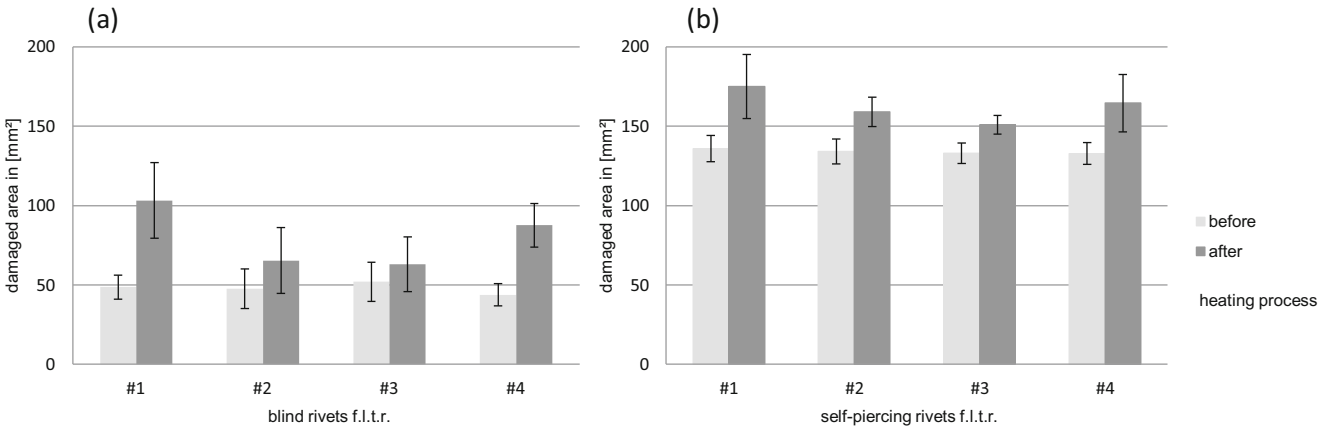

Fig. 6 Damaged area around the blind (**a**) and self-piercing rivets (**b**) before and after thermal loads were applied

among the four joints. The evaluation showed that blind rivets cause an initial crack formation that tends to expand in area and length when the joint is loaded. As measured values of damage length in main direction tend to scatter strongly, an approach based on single specimen analysis rather than a mean value approach was chosen. Investigations show that damage propagates not only in main stress direction, but in some cases also in opposite direction (see Fig. 7). However, in main stress direction, damage propagation is most visible, showing a longitudinal growth of about 60 % after thermal loads have been applied. Microsections underline the damage propagation that was detected in the C-Scan analysis. The images have been obtained with a Zeiss AxioImager M2m upright microscope at a magnification of 50x.

Self-piercing riveting in CFRP induces extensive plane defects. Before the specimens were exposed to high temperature, the damaged area showed a slightly rugged elliptic outline (see Fig. 5) where the stronger damage propagation in main fiber direction is already visible. Thermal expansion and resulting elongation on the outer joints caused insignificantly increased damage compared to the middle rivets. The processed ultrasonic images have shown that damage caused by self-piercing riveting behaves less sensitive on thermal loads than blind rivet defects due to a much greater initial injury of the CFRP. The initial damaged area offers less resistance to relative displacement, so that damage growth in case of crack-like initial damage in specimens with blind rivets is more prominent. An influence of fiber composite layup and main fiber orientation can also slightly be seen after damage growth, since the elliptic shape of the damage seems to be scaled in longitudinal and transversal direction through the applied loads (see Fig. 6). For self-piercing riveting, longitudinal damage scatters significantly less than for blind riveted joints since single cracks are less prominent. This behavior is also evident in Fig. 7, where damage dimensions in main fiber direction are depicted before and after the application of thermal loads. The image analysis reveals that damage can also propagate contrary to thermal stress direction, whereas main propagation takes place expanding the elliptic shape following the relative displacement. Increase in damaged area for self-piercing riveted joints is, in relation to the initial flaws, less distinctive. Total increase occurs in about the same range as for blind rivets. For the collected data, a cluster analysis has been performed focusing on the ratio of

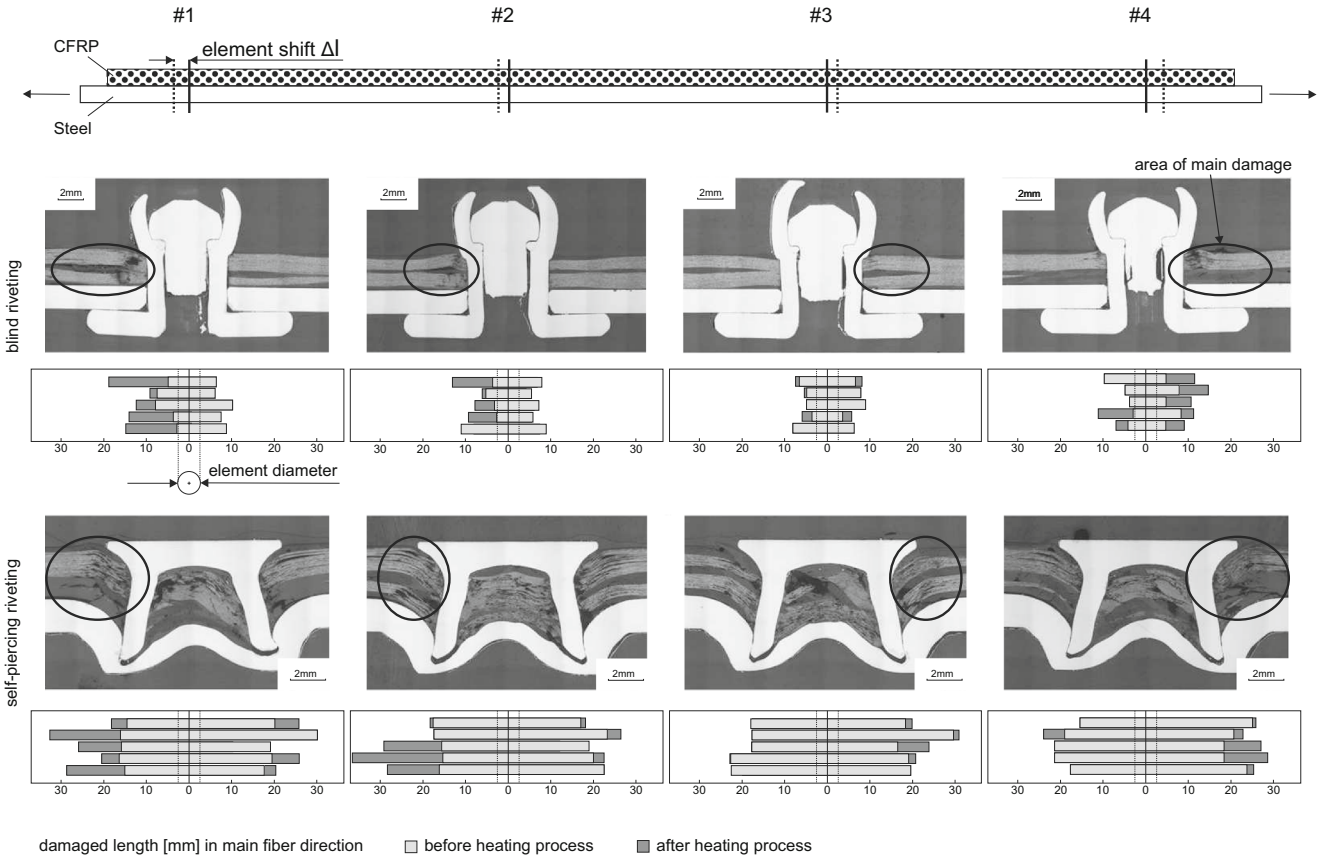

Fig. 7 Microsections of the damage distribution in 0°-direction relative to the rivet center for all four joints of the specimen after thermal loads were applied

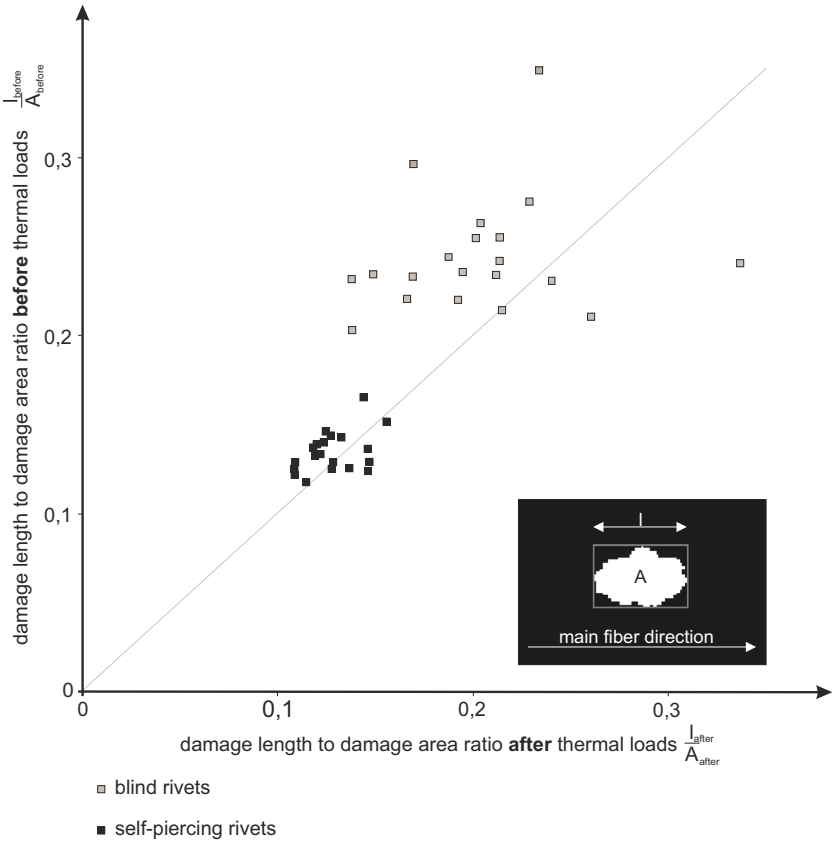

Fig. 8 Cluster analysis for the damage length to damage area ratio before and after thermal loads were applied

damage length in main fiber direction l to damage area A (see Fig. 8). A as well as l are measured with the image processing algorithm described in the Theory section. This ratio characterizes damage shape, where a low l/A ratio indicates a rather extensive damage form and higher l/A ratios describe crack-like defects. Therefore, crack-like damage induced by blind riveting results in higher values than extensive damage induced by self-piercing riveting. The cluster analysis underlines the dependency of damage propagation, due to thermal displacement, on pre-damage characteristics due to the two riveting processes. Crack-like damage tends to grow significantly in area as damage expands over the total crack length to extensive defects. Relatively, extensive defects grow less strongly although absolute damage growth is in about the same range as pre-damage is more extensive (see Fig. 8).

3.2 Shear tension tests

Conducted shear tension tests showed a significant drop in ultimate strength for specimens that were treated by a thermal process as described in chapter 2. For both blind riveting and self-piercing riveting, a similar drop in ultimate load of 1.30 and 1.77 kN from a nearly equal basis could be observed (see Fig. 9). The nature of the failure, however, was different for both joining techniques. Blind riveted specimens failed in bearing failure whereas specimens joined by self-piercing rivets failed in fastener pull-out due to decreasing interlock in the metal sheet. Based on the similar load drop, it is expected that despite the differing failure nature for both joining techniques the same mechanism is responsible for the loss in ultimate strength. For the specimens joined by self-piercing riveting, the connection itself rather than the material failed, by element pull out in the steel part. Therefore, a material degradation cannot be the source or at least not the single source for the drop in ultimate load. On the basis of [20], no influence of imperfections on ultimate strength under quasi-static loading should be expected. Based on this and independent test series, it is assumed that imperfections play a minor role regarding ultimate bearing strength. A possible explanation for the influence on design bearing strength but not ultimate bearing strength could lie in the fact that the element or bolt is pulled in areas which are not influenced by imperfections and which exhibit full strength. Under assumption of no influence of imperfections on ultimate bearing strength, a reduction of clamping pressure is the other remaining explanation for the drop in ultimate load after thermal

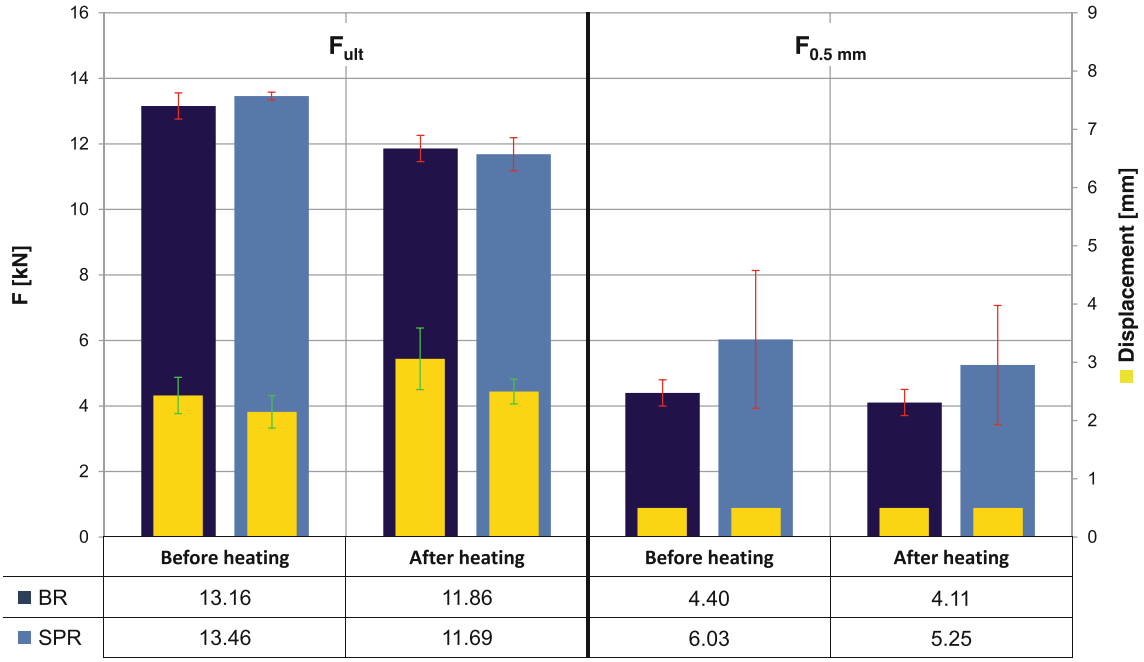

	Before heating	After heating	Before heating	After heating
BR	13.16	11.86	4.40	4.11
SPR	13.46	11.69	6.03	5.25

Fig. 9 Tension test results before and after heating for ultimate force and force at 0.5 mm displacement

treatment. An analysis of load at 0.5 mm displacement in the shear tension test showed that not only ultimate load is reduced, but also an overall lesser stiffness of the joints can be observed. In this context, stiffness is understood as the displacement up to ultimate force. As clamping pressure cannot be measured directly for both wire draw blind riveting and self-piercing riveting due to deformation in the joint and high joining forces, the friction force F_f is measured directly. This is possible for blind riveting under use of oversized pre-holes such as to avoid form closure. Friction force was determined for single point specimens in shear tension testing before and after heating as mean value in the force-displacement diagram between 0.4 and 0.7 mm displacement such as to avoid instabilities at the beginning of the test. Friction force was in average observed to be $F_{f,before} = 445\ N$ before and $F_{f,after} = 310\ N$ after heating. Transferred to the specimen geometry of Fig. 2 with four elements, this accumulates to a loss of 540 N in friction force due to heating, as shown in Fig. 10. The loss in ultimate force for blind riveted specimens, as shown in Fig. 9, in which not only heating but also thermal expansion occurs, however, exceeds this loss by 760 N. This is possible for blind riveting under use of oversized pre-holes such as to avoid form closure [24]. It is assumed that this additional loss in ultimate force can be explained by an increased loss in clamping and therefore friction force following the propagation of initial damage at hole edge during thermal expansion (see Fig. 10). In conclusion, it can be said that although imperfections play a minor role regarding ultimate bearing strength, their propagation leads to a decrease in clamping force and therefore ultimate force. The authors are convinced that the same mechanism is responsible for the loss in ultimate force for specimens joined by self-piercing riveting. As there are no means to measure friction or clamping force for self-piercing riveting proof, however, is elusive.

Fig. 10 Friction force hypothesis for the loss in ultimate force due to the heating process for the blind riveted specimen

4 Conclusion

Damage propagation on riveted CFRP-steel structures under thermal loads was investigated. Different failure behavior was characterized using a new damage detection method based on a MATLAB algorithm. Concluding remarks based on the experimental findings are summarized as follows:

1. It has been proven that relative displacement due to thermal elongation leads to significant damage propagation around joints.
2. The automatic image processing and measurement has proven to be advantageous to define damaged areas and to enable an evaluation of direction depending damage propagation.
3. Initial damage shape has a significant influence on further growth of flaws.
   (a) Crack-like initial damage (high l/A ratio) caused by blind riveting tears up and propagates to roundish plane defects.
   (b) Initial extensive damage (low l/A ratio) due to self-piercing riveting expands uniformly in elliptic shape.
4. The relative displacement equivalent ΔL offers a simple calculable value to link the damage size and shape to the position of the joint on the specimen without considering stresses.
5. The observed loss in ultimate force in tension tests is attributed to a loss in clamping force due to thermal loads. This loss is assumed to be increased by an interaction between clamping force and imperfections in the CFRP.

Acknowledgments Wagner J and Wilhelm M wish to thank BMW Group for funding this research as part of their Engineering Doctorate. The authors also wish to thank their colleagues at BMW Group who supported this work and Schiller I for proof reading.

All authors declare that they have a financial connection to the organisation funding this research.

References

1. ASTM D5961/D5961M Standard test method for bearing response of polymer matrix composite laminates
2. Barnes T, Pashby I (2000) Joining techniques for aluminium spaceframes used in automobiles. J Mater Process Technol 99(1–3):72–79. doi:10.1016/S0924-0136(99)00361-1
3. Barron TH (1998) Generalized theory of thermal expansion of solids. In: Ho CY, Taylor RE (eds) Thermal expansion of solids, vol.4.ASM International, Materials Park and Ohio
4. Camanho P, Matthews F (1997) Stress analysis and strength prediction of mechanically fastened joints in frp: a review. Compos Part A 28(1):529–547
5. Chaplot SL, Mittal R, Choudhury N (2010) Thermodynamic properties of solids: Experiment and modeling. Wiley-VCH, Weinheim
6. Goswami S (2005) A finite element investigation on progressive failure analysis of composite bolted joints under thermal environment. J Reinforc Plast Compos 24(2):161–171. doi:10.1177/0731684405042958
7. Hahn O, Hufenbach W, Gude M, Kläger O (2004) Entwicklung eines auslegungskonzepts fürgeklebte und genietete cfk/alkarosseriestrukturen auf basis experimenteller und numerischer untersuchungen. In: Freundeskreis LWF Universität Paderborn e.V. (ed) Mechanisches Fügen und Kleben
8. Hart-Smith LJ (1987) Design and empirical analysis of bolted or riveted joints. In: Matthews FL (ed) Joining fibre reinforced plastics. Elsevier Applied Science Publishers, Barking, pp 227–270
9. He X, Pearson I, Young K (2008) Self-pierce riveting for sheet materials: State of the art. J Mater Process Technol 199(1–3):27–36. doi:10.1016/j.jmatprotec.2007.10.071
10. Kim R, Whitney J (1976) Effect of temperature and moisture on pin bearing strength of composite laminates. J Compos Mat 10(2):149–155. doi:10.1177/002199837601000204
11. Kim YG, Lee DG (1998) Influence of fabrication residual thermal stresses on rubber-toughened adhesive tubular single lap steel-steel joints under tensile load. J Adhes 65(1–4):163–185. doi:10.1080/00218469808012244
12. Kim YG, Lee SJ, Lee DG, Jeong KS (1997) Strength analysis of adhesively-bonded tubular single lap steel-steel joints under axial loads considering residual thermal stresses. J Adhes 60(1–4):125–140. doi:10.1080/00218469708014414
13. Kochan A (2012) Untersuchungen zur zerstörungsfreien Prüfung von CFK-Bauteilen für die fertigungsbegleitende Qualitätssicherung im Automobilbau,Shaker,Aachen
14. Lee SJ, Lee DG (1995) Optimal design of the adhesively-bonded tubular single lap joint. J Adhes 50(2–3):165–180. doi:10.1080/00218469508014364
15. Persson E, Eriksson I, Zackrisson L (1997) Effects of hole machining defects on strength and fatigue life of composite laminates. Compos Part A 28(2):141–151. doi:10.1016/S1359-835X(96)00106-6
16. Reedy E, Guess T (1996) Butt joint strength: Effect of residual stress and stress relaxation. J Adhes Sci Technol 10(1):33–45. doi:10.1163/156856196X00436
17. Richter, F (ed) (1974) Die wichtigsten physikalischen Eigenschaften von 52 Eisenwerkstoffen, vol. 5, 1 edn.Verlag Stahleisen, Düsseldorf. doi:10.1002/mawe.19740050419
18. Sadowski T, Kneć M, Golewski P (2010) Experimental investigations and numerical modelling of steel adhesive joints reinforced by rivets. Int J Adhes Adhes 30(5):338–346. doi:10.1016/j.ijadhadh.2009.11.004
19. Thoppul SD, Finegan J, Gibson RF (2009) Mechanics of mechanically fastened joints in polymer–matrix composite structures—a review. Compos Sci Technol 69(3–4):301–329. doi:10.1016/j.compscitech.2008.09.037
20. Tönshoff H, Kaak R, Christoph G, Mester O (1999) Festigkeitsverhalten blindgenieteter fvk/stahl-verbindungen. VDI-Z 10(9):58–60. http://www.vdi-z.de/vdi-z/article.php?data[article_id]=14398

21. Tsao C, Hocheng H (2005) Computerized tomography and c-scan for measuring delamination in the drilling of composite materials using various drills. Int J Mach Tool Manufact 45(11):1282–1287. doi:10.1016/j.ijmachtools.2005.01.009
22. Walker SP (2002) Thermal effects on the pin-bearing behavior of im7/peti5 composite joints. J Compos Mat 36(23):2623–2651. doi:10.1177/002199802761675557
23. Wilhelm M, Füssel U, Nancke T, Duschl M (2013) Herausforderung cfk-stahl-mischbau: Quantifizierung von delaminationen infolge des umformtechnischen fügens (06.-08.05). http://jt2013.dgzfp.de/
24. Wilhelm MF, Fuessel U, Richter T, Riemer M, Foerster M (2014) Analysis of the shear-out failure mode for cfrp connections joined by forming. Journal of Composite Materials